Formability analysis of sheet metals by cruciform testing

IOP Conf. Series: Journal of Physics: Conf. Series **896** (2017) 012003 doi:10.1088/1742-6596/896/1/012003

Formability analysis of sheet metals by cruciform testing

B Güler[1], K Alkan[1] and M Efe[1]

[1]Department of Metallurgical and Materials Engineering, Middle East Technical University, Ankara 06800, Turkey

E-mail: mefe@metu.edu.tr

Abstract. Cruciform biaxial tests are increasingly becoming popular for testing the formability of sheet metals as they achieve frictionless, in-plane, multi-axial stress states with a single sample geometry. However, premature fracture of the samples during testing prevents large strain deformation necessary for the formability analysis. In this work, we introduce a miniature cruciform sample design (few mm test region) and a test setup to achieve centre fracture and large uniform strains. With its excellent surface finish and optimized geometry, the sample deforms with diagonal strain bands intersecting at the test region. These bands prevent local necking and concentrate the strains at the sample centre. Imaging and strain analysis during testing confirm the uniform strain distributions and the centre fracture are possible for various strain paths ranging from plane-strain to equibiaxial tension. Moreover, the sample deforms without deviating from the predetermined strain ratio at all test conditions, allowing formability analysis under large strains. We demonstrate these features of the cruciform test for three sample materials: Aluminium 6061-T6 alloy, DC-04 steel and Magnesium AZ31 alloy, and investigate their formability at both the millimetre scale and the microstructure scale.

1. Introduction

The forming abilities of materials can be tested under different loading conditions such as uniaxial tension, equibiaxial tension, plane strain, pure shear, etc [1]. Although uniaxial tension is most common testing method, it may underestimate the formability in a practical forming operation while multi-axial deformation analyses best represent the real sheet forming behaviour [2]. Bulge test, biaxial tensile test, Marciniak test and Nakajima test can access large strains and multi-axial loading paths compared to the uniaxial tension. However, these methods other than the biaxial tensile test, have significant limitations such as bending effect, friction effect, non-homogeneous material flow, presence of early necking, out-of-plane deformation, large-scale application etc. In cruciform biaxial tension testing, collection of the stresses at the centre of the specimen [3] and achieving large stresses and strains at the centre remain to be issues. As a solution, due to the various cruciform designs existing in the literature, the international standard ISO 16842:2014 standardize cruciform biaxial tension test [4]. However, the shape in this standard is not useful for achieving large strain since high strain is not obtained at the sample centre [5].

Large strain capability and strain path flexibility of cruciform biaxial tests are also useful for small-scale (microstructure scale) testing of materials which have deformation mechanisms sensitive to their unique microstructural features. Studies focusing on local deformation behaviour of lightweight metals such as aluminium, magnesium and titanium alloys have shown that microscale deformation alters the macro-scale behaviour [6-8]. As a result, these materials may have complex forming behaviour

compared to regular steels [9] and their forming ability should be studied at the small-scale. The cruciform design indicated in the standard is not suitable for micro-scale investigation due to large dimensions (240 mm in length).

In this research, we introduce a portable and easy to use biaxial test apparatus which is suitable for both macroscale and microscale testing. By successful specimen and testing conditions, uniform large strain distributions are obtained up to centre fracture. In addition, deformation mechanisms of three different metals under equibiaxial tension conditions and their relations with microstructural features are demonstrated and compared. Thus, the formability behaviours of three different materials are investigated and compared at both macroscale and microscale.

2. Materials and Methods

Aluminium 6061-T6, DC-04 steel and Magnesium AZ31 were selected as the sample materials having relatively different formability in order to investigate the effect of microstructural features on the deformation mechanisms. These materials have 0.11, 0.21 and 0.13 as strain hardening exponents (*n*) in their rolling direction, respectively. The cruciform sample design shown in figure. 1(a) is originated from [10] and further improvements were conducted to obtain maximum strain at the centre. The reduced thickness region (pit) shown in figure 1(a) was drilled by means of a CNC milling machine, resulting in good surface finish and smooth test region. The roughness of 2 mm test region was measured as Ra ≈ 2 µm for the materials.

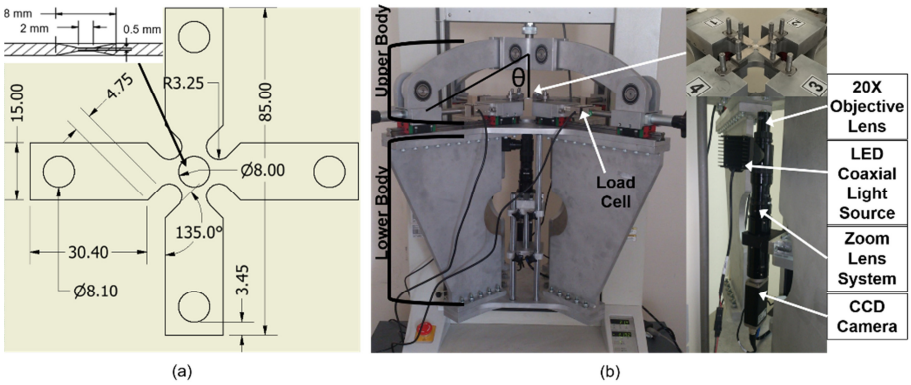

Figure 1. (a) Dimensions of Cruciform Sample (in mm); (b) Biaxial test setup

A portable, easy to use biaxial test apparatus shown in figure 1(b) was used to conduct cruciform biaxial tests. This apparatus was attached to Shimadzu Bending Test Machine with a capacity of 10 kN and the whole apparatus was designed to be portable and can be attached to any universal uniaxial, compression, bending test machine. When compression load is applied, this apparatus distribute the load to four arms with respect to the angle between the arm and vertical axis. Each axis of the loading mechanism moves independently on a rail and they are all connected to load cells. Horizontal load on each axis can be controlled by adjusting the angle between the horizontal axis and vertical arms that are connected to the test machine, as $F_{on\,axis} = (F_{machine} \times \tan\theta)/4$. In equibiaxial condition, load difference between each horizontal arm is less than 100 N.

To measure strain distributions, two dimensional digital image correlation (2D DIC) technique was used since it is a fast and precise method for measuring in-plane deformation and displacement fields of plastically deforming materials [11]. An open source, Ncorr v1.2, a MATLAB-based program, was used for the 2D-DIC. Both macroscale and microscale analysis were conducted at 3X and 20X, respectively. For macroscale DIC, the subset size and step size were adjusted as 80 and 8 pixels, respectively while for microscale DIC they were adjusted as 70 and 7, respectively. The corresponding spatial resolutions were 1.2 µm/pixel and 0.18 µm/pixel for macroscale and microscale DIC, respectively. The maximum strain error calculated by rigid body translation was 0.14% and the

measured Green-Lagrangian strains from the DIC were converted to the true strains by means of following formula:

$$\varepsilon = \ln(\sqrt{2E + 1}) \quad (1)$$

where E and ε are Green-Lagrangian and true strains, respectively.

The test setup allowed both microscale and microscale investigation in a single test by means of interchangeable objectives and the zoom lens setup. Since the aim was to investigate the strain localizations at the microscale, a preliminary macroscale analysis was conducted to determine the location of strain localizations. At first, sample was deformed until the first signs of plastic deformation. Then, the test was paused and the 2D-DIC was conducted to map the strain distributions. After pinpointing the strain localized regions, objectives and the lens setup were reconfigured for the microscale analysis and zoomed to the localizations. Test was resumed and the strains were mapped at the microstructure scale with the increased resolution. The average plastic strain obtained in the previous macroscale analysis was added to the new results.

3. Results and Discussion

3.1. Strain distributions at the macroscale

To obtain large strains at the centre, the design of the cruciform sample and the pit take an important role [12]. The most important parameter in the pit design is the thickness reduction ratio, which increases the chances of centre fracture [13]. We preferred single reduction for simple manufacturing and our maximum reduction was 75% corresponding to 0.5 mm thickness. Centre region became delicate and fragile below 0.5 mm thickness. Due to the reduced thickness and the tapered profile of the pit (figure 1(a)), the samples failed or cracked from the centre.

As centre fracture was possible in the sample with tapered-profile pit, we proceeded to the strain analysis in the test region. Figure 2 shows the distribution of the principal strains just before the fracture under equibiaxial tension. Except the magnesium, samples deform with strain bands crossing at the sample centre [14]. These bands originate from the unique geometry and deformation characteristics of the cruciform samples. The bands link the opposite diagonal corners and cross each other at the centre. There are also shear deformation and inhomogeneous localized areas along the bands while the shear strains approach to zero at the centre, providing relatively uniform deformation. As the shear strains are not zero, the whole pit region should not be considered as the test region even if the median true strains are balanced under equibiaxial tension test. The true equibiaxial condition is achieved at the centre within a circular area having 1 mm diameter and this location is selected as the test area shown in figure 2 since shear strain should be minimum in equibiaxial tension condition [15]. The principal strains are maximum at the 1 mm-diameter test region while the shear strains are approximately zero. Median true principal strains in this region are calculated as ε_1 = 0.16 and ε_2 = 0.14 for Al 6061-T6, ε_1 = 0.34 and ε_2 = 0.30 for DC-04 Steel and ε_1 = 0.08 and ε_2 = 0.08 for Magnesium AZ31, resulting in an equivalent strain ($\bar{\varepsilon}$) of 0.3, 0.64 and 0.16, respectively. The equivalent strains were calculated by the following formula:

$$\bar{\varepsilon} = \sqrt{\frac{2}{3}\{\varepsilon_1^2 + \varepsilon_2^2 + \varepsilon_3^2\}} \quad (2)$$

For aluminium and steel, $\bar{\varepsilon}/n$ ratio of ~ 3 confirms the large strain capability of the cruciform test [14]. Therefore, the two intersecting strain bands maximize the principal and equivalent strains at the centre and promote fracture at the same location. Outside the bands, the equivalent strains are lower and close to the strain hardening exponent of the material.

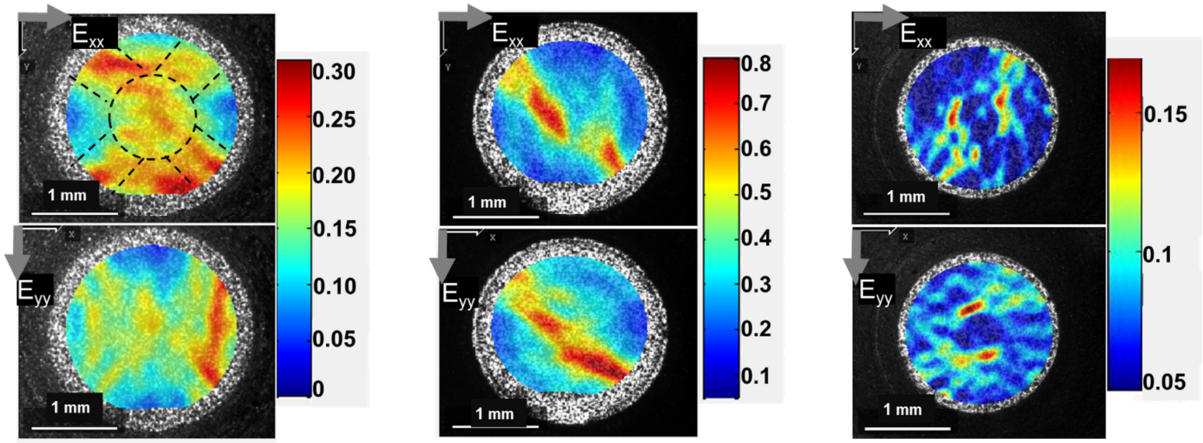

Figure 2. DIC Results of (a) Al 6061-T6, (b) DC-04 Steel and (c) Mg AZ-31up to fracture. The upper results for E_{xx} while the below for E_{yy}. The strain bands are shown as dashed lines on Al 6061-T6 results. For DC-04 steel one strain band is dominant onset of fracture while no strain bands are shown for Mg AZ-31

A detailed imaging of the fractured samples within a scanning electron microscope (SEM) suggests that the strain bands may originate from the corners (figure 3(b)). Together with the pit, the corners may deform uniformly until the overall strain reaches *n*. After this, necks form at all corners and strain bands connect them. As strain bands intersect each other at the centre, this region continues to deform under equibiaxial tension and reaches large equivalent strains. This mechanism is schematically depicted in figure 3(a) and confirmed by the SEM picture of Aluminium in figure 3(b). Surface protrusions are concentrated in the strain bands and the centre, while the rest of the sample remains undeformed. Indeed any cruciform geometry can develop this type of strain distribution, as the stress concentration at the corners is unavoidable. In our case, the strain bands were distinct due to the small-scale of the samples, where the width of strain bands is nearly 1 mm, same as the diameter of test region.

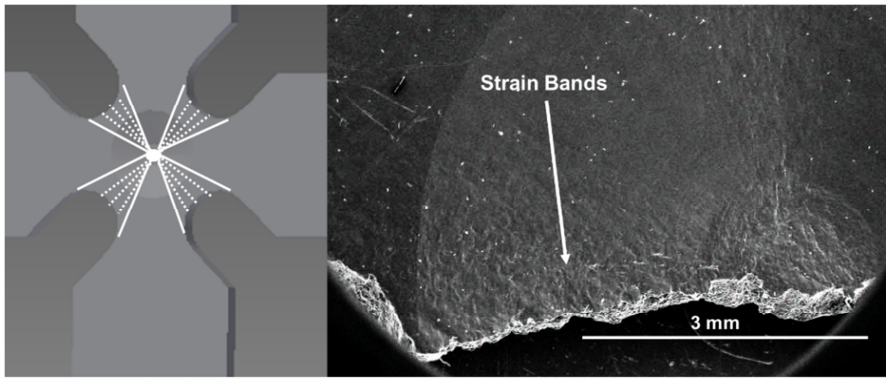

Figure 3. (a) Schematic drawing of the sample and strain bands; (b) SEM image of Al showing the location of the strain bands. Surface protrusions are visible in the strain bands and at the centre confirming the plastic deformation of these regions.

On the other hand, during deformation of magnesium, strain bands are not observed. Since magnesium deformation is highly related to its microstructure, uniform deformation is unlikely, resulting in several strain localized spots instead of the strain bands. Figure 2(c) shows the strain

localized regions before the onset of fracture. Although strain bands are absent, strain localizations still occur within the 1-mm-diameter-region. The localized deformation in magnesium at the macroscale proves the necessity of microscale investigations.

3.2. Microscale investigation of deformation

Under the equibiaxial loading, grains of both Al 6061-T6 and DC-04 Steel are deformed randomly as expected from isotropic materials. In addition, strain is localized at some grain boundaries which lead to the onset of crack formation. In the Al 6061-T6, randomly deformed grains are expanded during deformation, which inhibit deformation at their neighbouring grains (figure 4(a), dashed arrows). These expansions of deformed grains indicate that the neighbouring grains are not free to expand as the boundaries of deformed grains restrict their movement. Cracks initiate at the boundaries of these deformed grains (figure 4(a), solid arrow). Thus, some grains have high strain values while the other grains surrounded by highly deformed grains have limited deformation and strain.

In the DC-04 steel sheet, the deformation of grains do not vary from each other significantly. Comparing to Al 6061-T6, relatively uniform deformation is observed among various grains. However, strain is still localized to the grain boundaries, followed by the crack initiation (figure 4(b)). After the crack initiations, strain values increase at the boundaries, while rest of the grains deform uniformly.

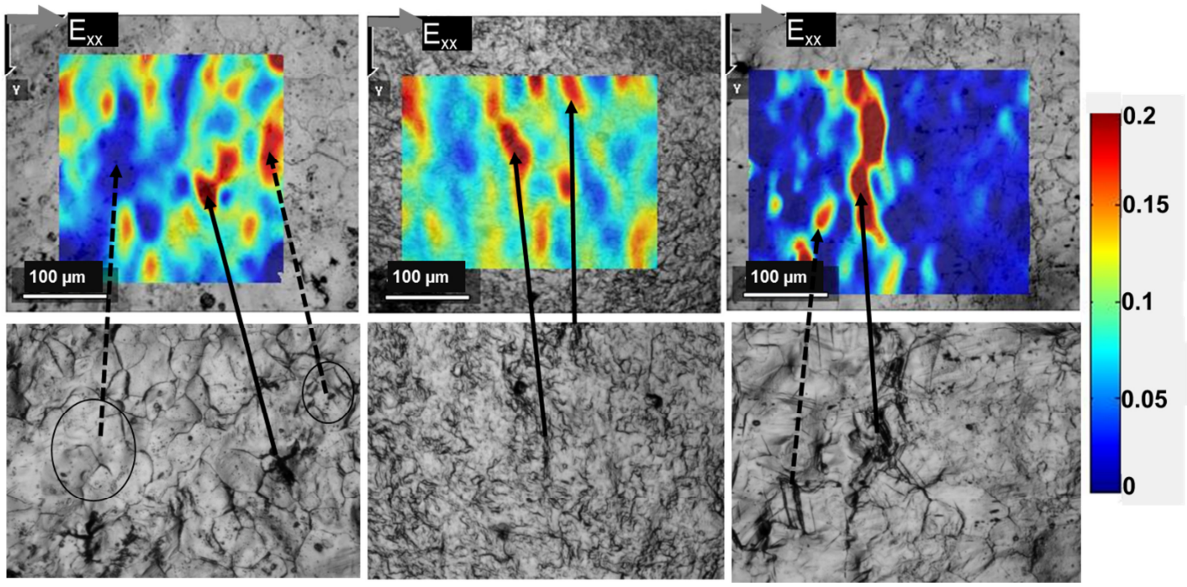

(a) (b) (c)

Figure 4. Microscale DIC results showing deformation mechanisms of (a) Al 6061-T6, (b) DC-04 Steel, (c) Mg AZ31.

In the Mg AZ31, different strain localization mechanisms take place as it is a relatively brittle material due to the HCP crystal structure. There are two well-known deformation mechanisms in magnesium alloys at room temperature: dislocation slip along basal planes and twinning. In small grain sized materials, the dominant mechanism is slip, which can travel across the thickness of the sample to form a localized neck. On the other hand, in large grain sized alloys, twin band formation is favourable. The existence of both large and small grains can trigger both slip and twin bands mechanism so larger stains can be achieved [16]. In our material, there are both large and small grains. At the early stages of deformation, the twin bands are observed under the equibiaxial loading (figure 4(c)). With increasing strain, the slip and twin bands occur simultaneously. Consequently, the cracks start at both twin band (figure 4(c), solid arrow) and slip band (figure 4(c), dashed arrow).

4. Summary

The cruciform biaxial testing has a unique deformation mechanism which favours large and uniform strains at the test region. In addition, it is possible to investigate the microscale deformation mechanisms. Both the DC-04 steel and the Al 6061-T6 alloy deform uniformly at the macroscale and reach a high ratio of equivalent strain to the strain hardening exponent. For aluminium, the microscale deformation is quite heterogeneous as some group of grains remain undeformed. Strain localizes the grain boundaries between the deformed and undeformed grains, followed by the crack initiation and fracture at the localized regions. For an anisotropic material such as magnesium, deformation behaviour is highly related to the grain size. Limited deformation provided by slip or twin bands result in strain localizations and eventually crack initiation. Thus, for materials having microstructure sensitive deformation behaviour, microscale strain analyses can yield important clues about the deformation and fracture behaviour and the cruciform test setup with dedicated sample design allows microscale investigations until the fracture.

Acknowledgments

This work was supported by European Commission's Research Executive Agency's Marie Curie Actions–Career Integration Grant (FP7-PEOPLE-2013-CIG) with grant agreement #631774. We would like to thank Berkay Bayramin for his help in the sample preparation and testing.

References

[1] Banabic D 2009 *Sheet Metal Forming Processes* (Berlin: Springer)
[2] Li D and Ghosh A 2004 *J. Mater. Process. Technol.* **145** 284
[3] Hannon A and Tiernan P 2008 *J. Mater. Process. Technol.* **198** 1
[4] Song X, Leotoing L, Guines D and Ragneau E 2016 *Eng. Fract. Mech.* **163** 130
[5] ISO 16842:2014. Metallic materials-sheet and strip-biaxial tensile testing method using a cruciform test piece.
[6] Tong W 1998 *J. Mech. Phys. Solids* **46** 2087
[7] Aydıner C C and Telemez M A 2014 *Int. J. Plast.* **56** 203
[8] Efstathiou C, Sehitoglu H and Lambros J 2010 *Int. J. Plast.* **26** 93
[9] Kleiner M, Geiger M and Klaus A 2003 *CIRP Ann-Manuf. Techn.* **52** 521
[10] Abu-Farha F, Hector L G Jr and Khraisheh M 2009 *JOM* **61** 48
[11] Manya M, Hector L G, Verma R and Tong W 2006 *Mater. Sci. and Eng. A* **418** 341
[12] Hannon A and Tiernan P 2008 *J. Mater. Process Technol.* **198** 1
[13] Tasan C C, Hoefnagels J P M, Dekkers E C A and Geers M G D 2012 *Exp. Mech.* **52** 669
[14] Seymen Y, Güler B and Efe M 2016 *Exp. Mech.* **56** 1519
[15] Hu J, Marciniak Z and Duncan J 1992 *Mechanics of Sheet Metal Forming* (London: Edward Arnold)
[16] Mishra S K, Tiwari S M, Carter J T and Tewari A 2014 *Mater. Sci. and Eng. A* **599** 1